ICA 2019 AACHEN

PROCEEDINGS of the
23rd International Congress on Acoustics

9 to 13 September 2019 in Aachen, Germany

Sound Absorption Characteristics of a Back-Perforated Honeycomb Panel with an Air-Layer

Kyungsoo KONG[1]; Tetsuya SAKUMA[2]; Naohisa INOUE[3]

[1 2 3] University of Tokyo, Japan

ABSTRACT

A honeycomb panel has a high potential in noise control engineering as well as in any other engineering fields. This paper demonstrates that a Back-Perforated Honeycomb Panel(BPHP) placed with a back air-layer exhibits unique absorption characteristics composed of the combination of panel- and resonator-type mechanisms. A BPHP is theoretically modeled as a two-mass system composed of panel and resonator's neck masses, and multiple air stiffness. First, resonance mechanisms are clarified from the model. It is revealed that the panel-type resonance can arise from the panel mass and air stiffness corresponding to the total thickness of the panel and air-layer, even if a BPHP is placed considerably closely to the back wall. Next, normal- and random- incidence absorption coefficients are calculated with changing several parameters such as perforation diameters, hole pitches, panel thickness, back air-layer thickness and so on. Furthermore, a supplementary numerical calculation confirms the validity of the proposed theoretical model. Through the case studies, several charts are arranged for effective design of BPHPs as low-frequency sound absorber.

Keywords: Sound absorbing material, Sound absorption coefficient, Honeycomb panel, Perforated plate

1. INTRODUCTION

With the expansion of acoustic design, a variety of acoustic materials have been actively developed for high performance, lightness, durability, weather resistance, recycling and so on. One of such materials is a honeycomb plate (sandwich panel having a honeycomb core) that possesses lightweight and high rigidity at the same time. This feature is advantageous for structural or exterior materials in various fields such as transport vehicle, construction and so on. In the field of acoustics, there have been various utilizations proposed based on interesting mechanisms and ideas. For instance, a honeycomb cores are used as the wave guide in the double-leaf panels [1,2], which leads to increase of the insulation performances. Another implementation is that a Helmholtz resonator is composed by replacing the one surface of a honeycomb sandwich panel by a micro-perforated plate(MPP) [3]. The latter is becoming a practical use because it can be easily realized by perforating the plate surface of the honeycomb plate instead of using MPP. This type panel is noted PHP in the following.

PHP is usually installed with the perforated surface facing the indoor side to make use of resonator-type absorption. On the other hand, the authors have found that when PHP is installed with an air layer directing its perforated side to the air layer side, a unique sound absorption characteristic can be obtained by the composite mechanism of the resonator type and plate vibration type. We named this structure as Back-Perforated Honeycomb-Panel (BPHP). This paper presents a simple theoretical model based on a lumped parameter system to calculate the absorption coefficient for BPHP. Based on this model, resonance mechanisms and absorption characteristics are clarified in detail. The proposed model is also validated by the numerical analysis. Finally, through the case studies, several charts are arranged for effective design of BPHPs as low-frequency sound absorber.

[1] 4709384469@edu.k.u-toyko.ac.jp [2] sakuma@k.u-tokyo.ac.jp [3] inoue@env-acoust.k.u-tokyo.ac.jp

2. THEORETICAL ANALYSIS

2.1 Formulation

Figure 1 shows the definition of various parameters and the lumped constant model. The equations of motion to the whole of PHP and to the neck mass are given by the following Eqs. 1 and 2, respectively. The continuity condition between the normal particle velocity of incidence field and the vibration velocity of the PHP is given by Eq. 3.

$$m_{\mathrm{n}}\ddot{x}_{\mathrm{n}} + k_{\mathrm{sn}}(x_{\mathrm{n}} - x_{\mathrm{s}}) + k_{\mathrm{scn}}x_{\mathrm{s}} + k_{nc}x_{\mathrm{n}} + c_{\mathrm{sn}}(\dot{x}_{\mathrm{n}} - \dot{x}_{\mathrm{s}}) = 0 \tag{1}$$

$$m_{\mathrm{s}}\ddot{x}_{\mathrm{s}} + k_{\mathrm{sn}}(x_{\mathrm{s}} - x_{\mathrm{n}}) + k_{\mathrm{scn}}x_{\mathrm{n}} + k_{sc}x_{\mathrm{s}} + c_{\mathrm{sn}}(\dot{x}_{\mathrm{s}} - \dot{x}_{\mathrm{n}}) = P_{\mathrm{i}} + P_{\mathrm{r}} \tag{2}$$

$$\frac{\cos\theta}{\rho_0 c_0}(P_{\mathrm{i}} - P_{\mathrm{r}}) = \dot{x}_{\mathrm{s}} \tag{3}$$

where P_{i} and P_{r} are the incident and reflected wave amplitude, respectively. m_{s} is the area density of PHP. m_{n} is the effective area density of the neck, and c_{sn} is the viscous damping coefficient of the neck, which is given as follows based on the Allard–Ingard model as follows.

$$\phi_{\mathrm{t}} = \frac{S_{\mathrm{n}}}{S_{\mathrm{t}}}, \phi_{\mathrm{h}} = \frac{S_{\mathrm{n}}}{S_{\mathrm{h}}}, \varepsilon = \frac{8r}{3\pi}(1 - 1.25\sqrt{\phi_{\mathrm{t}}}),$$

$$m_{\mathrm{n}} = \rho_0\phi_{\mathrm{t}}(l_{\mathrm{n}} + 2\varepsilon), c_{\mathrm{sn}} = R_{\mathrm{v}}\phi_{\mathrm{t}}\left(\frac{2l_{\mathrm{n}}}{r} + 4\right), R_{\mathrm{v}} = \frac{\sqrt{2\eta\rho_0\omega}}{2},$$

where S_{n} is a hole area, and S_{t}, S_{h} is a honeycomb area of internal and external measure, respectively. r and l_{n} are hole radius and neck length. η and ρ_0 are viscosity coefficient and density of air. The stiffness constants k_{sn}, k_{nc}, k_{scn} and k_{sc} are expressed as follows.

$$k_{\mathrm{s}} = \frac{\rho_0 c_0^2}{L_{\mathrm{s}}}, k_{\mathrm{s}} = \frac{\rho_0 c_0^2}{L_{\mathrm{c}}\cos^2\theta}, k_{\mathrm{sn}} = \phi_{\mathrm{t}}\phi_{\mathrm{h}}k_{\mathrm{s}}$$

$$k_{\mathrm{sc}} = (1 - \phi_{\mathrm{t}})^2 k_{\mathrm{c}}, k_{\mathrm{scn}} = (1 - \phi_{\mathrm{t}})\phi_{\mathrm{t}}k_{\mathrm{c}}, k_{\mathrm{nc}} = \phi_{\mathrm{t}}^2 k_{\mathrm{c}}$$

where c_0 is the speed of sound. The stiffness constants are reasonably approximated because the dimensions of each part are sufficiently smaller than the wavelength. It should be noted that the above-mentioned inertia and resistance corrections are derived for the hole on the motionless baffle. Therefore, the validity of using these corrections will be verified in the next section in comparison with the detailed model by numerical analysis. In this paper, unit amplitude incident sound pressure (P_{i} = 1) is given, and the simultaneous equation of Eqs. 1 to 3 is solved by the direct method to calculate the complex reflectance.

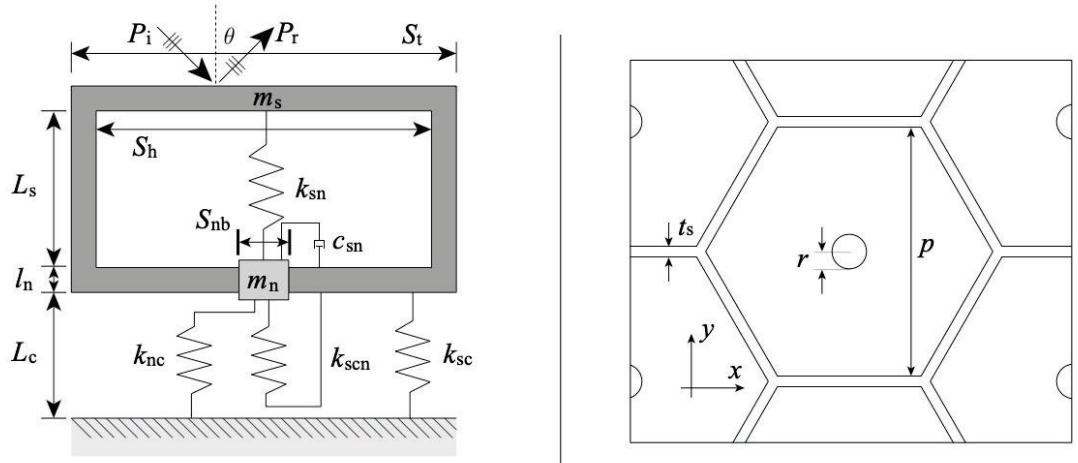

(a) A Theoretical model of the Perforated Honeycomb Panel

(b) Cross-section of the Perforated Honeycomb Panel

Figure 1 – Problem settings for the theoretical calculation of absorption coefficients of a BPHP.

2.2 Resonance Mechanism and Frequencies

The BPHP system without damping and under free vibration is given as the matrix form as follows.

$$\begin{bmatrix} k_{\mathrm{sn}} + k_{\mathrm{sc}} - \omega^2 m_{\mathrm{s}} & -k_{\mathrm{sn}} + k_{\mathrm{scn}} \\ -k_{\mathrm{sn}} + k_{\mathrm{scn}} & k_{\mathrm{sn}} + k_{\mathrm{nc}} - \omega^2 m_{\mathrm{n}} \end{bmatrix} \begin{Bmatrix} x_{\mathrm{s}} \\ x_{\mathrm{n}} \end{Bmatrix} = \begin{Bmatrix} 0 \\ 0 \end{Bmatrix}$$

Two resonance frequencies of this system are obtained as the frequency at which the determinant of the left side matrix becomes 0. Hereinafter, these frequencies will be referred to as f_{l} and f_{h} ($f_{\mathrm{l}} < f_{\mathrm{h}}$), respectively. Figure 2 shows the changes of the resonant frequency f_{l}, f_{h} with respect to the panel perforation ratio. The asymptotic curves obtained by approximation in terms of the perforation ratio are also shown. It can be seen that the equivalent resonance systems are different before and after a certain perforation ratio (ϕ').

$$\phi' = \sqrt{\frac{m_{\mathrm{n}}}{m_{\mathrm{s}}} \frac{L_{\mathrm{s}}}{L_{\mathrm{s}} + L_{\mathrm{c}}}} \tag{4}$$

In $\phi < \phi'$, two resonances are brought by the single resonator (f_{ll}) and by the plate resonance (f_{hl}) with L_{c} as an air layer. On the other hand, in $\phi < \phi'$, two resonances are brought by the resonator neck (mass) and two springs of the resonator cavity and the back air-layer (spring)(f_{hh}) and by the plate resonance with total air layer L_{s}+L_{c} (f_{lh}).

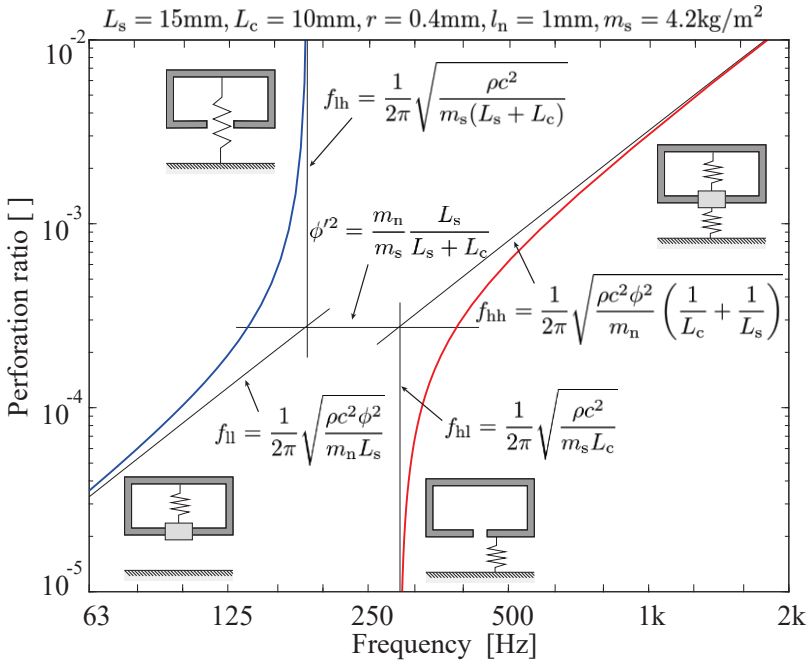

Figure 2 – Relation between the perforation ratio and eigen-frequencies of a BPHP.

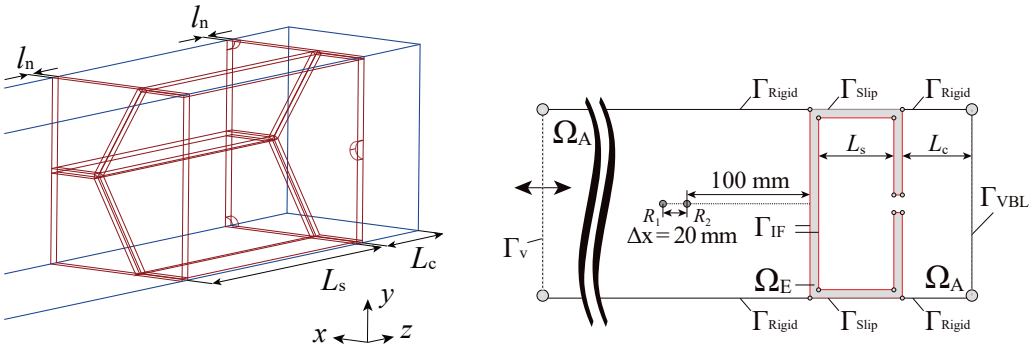

(a) Perspective (b) Domain notation

Figure 3 – Problem settings for the theoretical calculation of absorption coefficients of a BPHP.

3. COMPARISON WITH FINITE ELEMENT MODEL

3.1 Formulation of the Numerical Analysis

The finite element analysis is performed by setting an impedance tube problem as shown in Figure 3. The formulation of the analysis is briefly noted.

■ Acoustic Field : Let us consider the following weak-form of Helmholtz equation for the acoustic field in the impedance tube, resonator neck, back air-layer and cavity of the honeycomb panel.

$$\int_{\Omega_A} \nabla \delta p \cdot \nabla p \, dV - k^2 \int_{\Omega_A} \delta p p dV - \int_{\Gamma} \delta p \frac{\partial p}{\partial n} dS = 0 \tag{5}$$

where p and k are the sound pressure and wave number in the air, respectively. $\partial/\partial n$ denotes the outward normal derivative to the sound field.

■ Elastic body vibration field : Let us consider the following weak-form of the elastodynamic equation for the vibration field of the honeycomb plate.

$$\int_{\Omega_E} \delta \underline{\underline{\varepsilon}} : \underline{\underline{\sigma}} dV - \rho_E \omega^2 \int_{\Omega_E} \delta \mathbf{u} \cdot \mathbf{u} dV - \int_{\Gamma} \delta \mathbf{u} \cdot (\underline{\underline{\sigma}} \cdot \mathbf{n}) dS = 0 \tag{6}$$

where $\mathbf{u}$, ρ_E, ω, $\mathbf{n}$ are a three-dimensional displacement of an elastic body, density, angular frequency, and an outward vector with respect to an elastic body vibration field. $\underline{\underline{\varepsilon}}$, $\underline{\underline{\sigma}}$ is a strain tensor and a stress tensor, and each component is defined as follows.

$$\varepsilon_{ij} = \frac{1}{2}\left(\frac{\partial u_{x_i}}{\partial x_j} + \frac{\partial u_{x_j}}{\partial x_i}\right)$$

$$\sigma_{ij} = \lambda \mathrm{div}\mathbf{u}\delta_{ij} + 2\mu\varepsilon_{ij}, \delta_{ij} = \begin{cases} 1 & (i = j) \\ 0 & (i \neq j) \end{cases}$$

where λ, μ are Lamé's first and second parameters, respectively.

■ Boundary and Continuous conditions : It is essential for this problem to take the effect of the viscous boundary layer around the neck into account. Considering the influence of the translational motion of the panel, we give the following conditions at the boundary of the acoustic field.

$$\frac{\partial p}{\partial n} = \begin{cases} 0 & (\text{on } \Gamma_{\mathrm{Rigid}}) \\ -j\omega\rho_0 v_n & (\text{on } \Gamma_V) \\ -(j\omega)^{-1/2} c_V \nabla_{\tan}^2 p & (\text{on } \Gamma_{\mathrm{VBL}}) \\ \rho_0\omega^2[\mathbf{n}]\cdot\{\mathbf{u}\} - (j\omega)^{-1/2} c_V \nabla_{\tan}^2 p + (j\omega)^{3/2}\rho_0 c_V \nabla_{\tan} \cdot \left(\begin{bmatrix}\mathbf{t}\\ \mathbf{b}\end{bmatrix}\{u\}\right) & (\text{on } \Gamma_{IF}) \end{cases} \tag{7}$$

where $\mathbf{t}$, $\mathbf{b}$ and $\mathbf{n}$ are the tangent, binormal and principal normal vector of the local orthogonal coordinate system set on the boundary. v_n is the normal direction velocity of the vibratory boundary Γ_v, $\nabla_{\tan}$ is the nabla operator in the tangential plane, and c_V is the square root of the kinematic viscosity of air. On the other hand, the following conditions are considered at the elastic body vibration field boundary.

$$\underline{\underline{\sigma}} \cdot \mathbf{n} = \begin{cases} f_n \mathbf{n} & (\text{on } \Gamma_{\mathrm{Slip}}) \\ -p\mathbf{n} - (j\omega)^{3/2}\rho_0 c_V \begin{bmatrix}\mathbf{t}\\ \mathbf{b}\end{bmatrix}^T \begin{bmatrix}\mathbf{t}\\ \mathbf{b}\end{bmatrix}\{\mathbf{u}\} + (j\omega)^{-1/2} c_V \begin{bmatrix}\mathbf{t}\\ \mathbf{b}\end{bmatrix} \nabla_{\tan} p & (\text{on } \Gamma_{IF}) \end{cases} \tag{8}$$

Although the direct stress f_n determined by the deformation is unknown before analysis, the normal direction displacement on the slip boundary Γ_{Slip} is zero ($\mathbf{u} \cdot \mathbf{n} = 0$). So, the boundary integral term of Eq. 5 becomes zero.

■ Identification of the normal-incidence absorption coefficient : By using the transfer function method, the normal incidence absorption coefficient can be calculated from the sound pressure p_1, p_2 at two points R_1, R_2 shown in Fig. 3 (b).

$$\alpha_n = 1 - \left| \frac{p_2 - p_1 \exp(jk\Delta x)}{p_1 \exp(-jk\Delta x) - p_2} \right|^2$$

3.2 Comparison of Lumped Constant and Finite Element Models

The normal-incidence absorption coefficients are calculated for different hole radius r and back air-layer L_c. The following parameters are fixed: p = 20 mm, m_s = 4.2 kg/m^2, L_s = 30 mm, t_s = 0.5 mm, l_n = 1 mm. Figure 4 shows the results of the lumped constant model and the finite element model together with the resonance frequencies (f_{ll}, f_{lh}, f_{hl}, f_{hh}). Two peaks are observed in the absorption coefficient approximately around f_{lh} and f_{hh}. When the hole radius is 0.25 mm, the Helmholtz resonance frequency(f_{ll}) of the PHP unit becomes close to the plate resonance frequency(f_{lh}), and the peak frequencies of the absorption coefficient tend to shift to the low/high frequency range with respect to f_{lh}, f_{hh}, respectively. And it can be seen that f_{ll} and f_{lh} are closer as the back air-layer is thinner within the range of the aperture ratio $\phi < \phi'$ from the equation (4). The tendency of the results of the lumped parameter model agrees well with that of the finite element model in any conditions. However, under the condition of (a), (d) with a hole radius of 0.25 mm, the numerical analysis value has a smaller peak value of the absorption coefficient than the theoretical value, and the degree of shift with respect to f_{lh}, f_{hh} is also small. Under the the condition of (a), (d), since the diameter of the hole and the viscosity boundary thickness in the vicinity of f_{lh} are approximately the same, it is considered that both models include an error in the movement (inertia/ attenuation correction) of the neck air. In addition, the influence of the viscous boundary layer on the bottom surface of the acoustic tube (Γ_{VBL}) is relatively small when the thickness of the back air-layer is 1 mm.

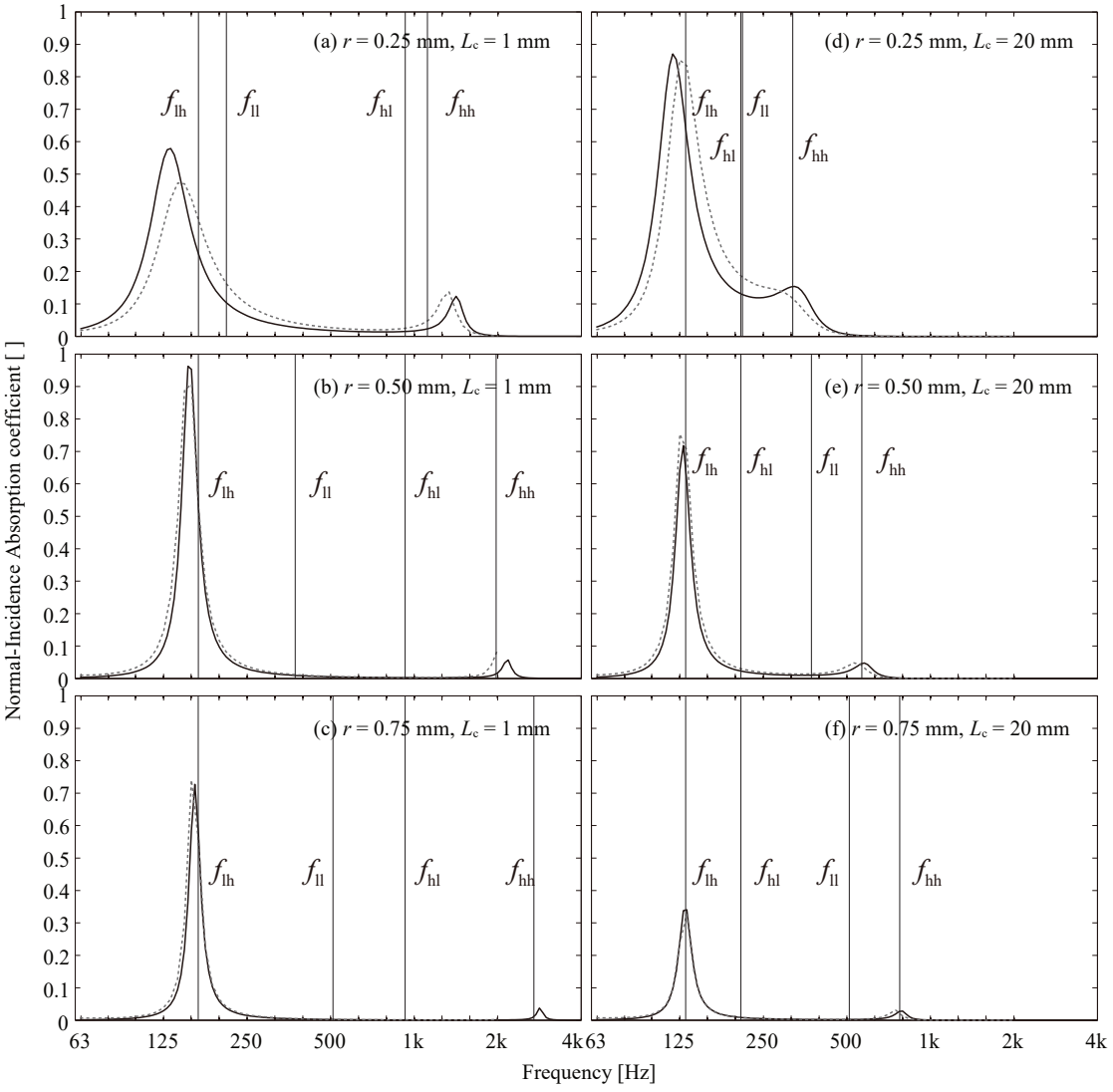

Figure 4 – Normal-incidence absorption coefficients calculated for the BPHP with different perforation radius and back air-layer thickness combinations.
Solid-black and dotted-gray lines calculated by the lumped-constant model and the finite element model, respectively. FEM results are shown up to 2 kHz.

4. PARAMETRIC STUDY

Since the validity of the lumped constant model has been shown in the previous section, this section discusses the basic characteristics and design method of BPHP based on the lumped constant model.

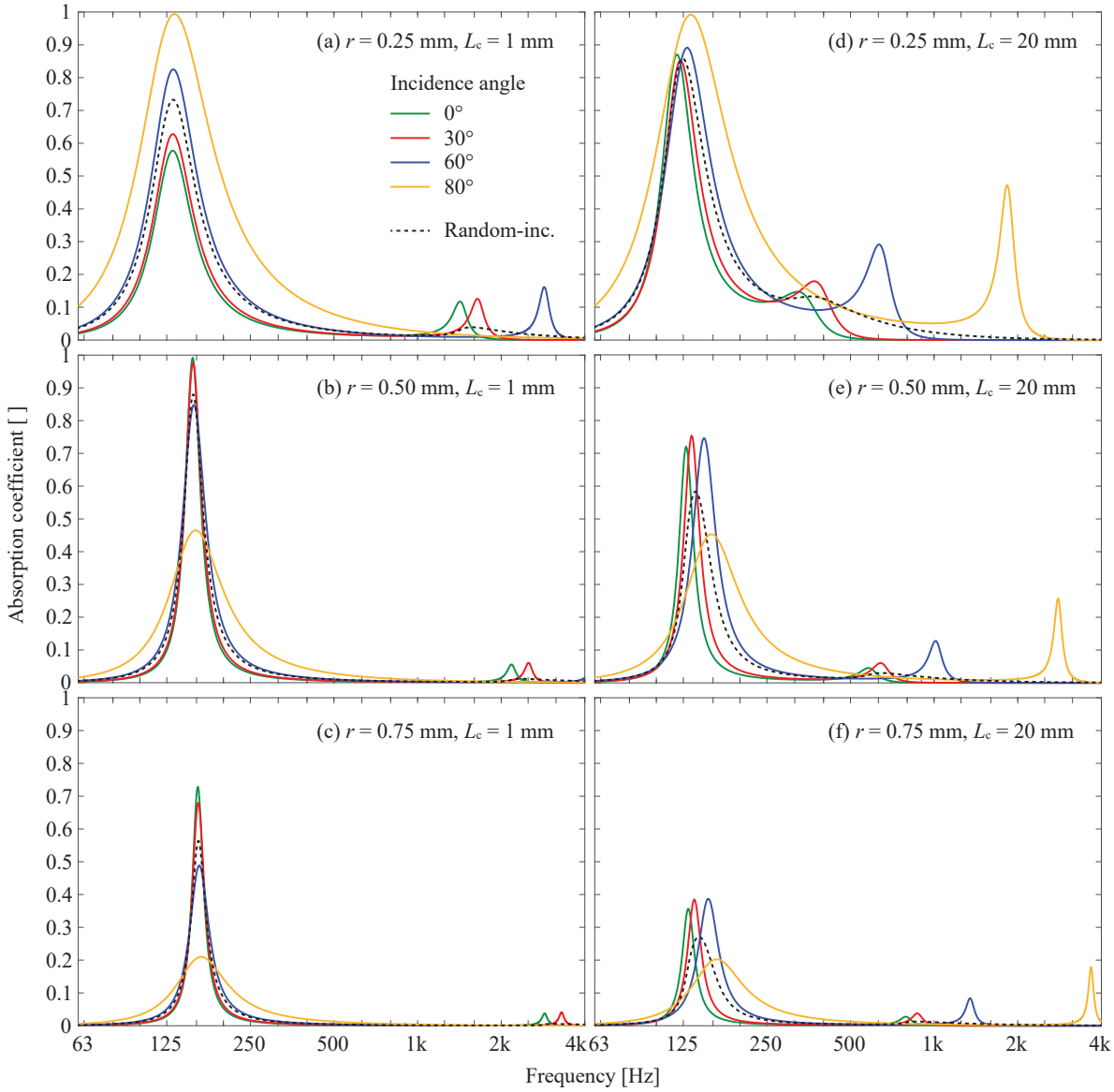

Figure 5 – Oblique- and random-incidence absorption coefficients calculated for the BPHP with different perforation radius and back air-layer thickness combinations.

4.1 Oblique- and random-incident absorption coefficients

The oblique- and random-incidence sound absorption coefficients were calculated under the same conditions as in Section 3.2. The random incident absorption coefficient was calculated by averaging the oblique incident absorption coefficients calculated at each incident angle based on the Paris equation. The results are shown in Figure 5.

Except for the resonance near f_{lh} in the back air-layer 1 mm (a ~ c), the spring constant k_c of the back air-layer increases with the increase of the incident angle, and the peak of the absorption coefficient shifts to the high frequency range. Because f_{lh} is substantially determined by the PHP thickness when the back air-layer is thin. On the other hand, when the back air-layer is thick, the degree of shift of the plate resonance also depends on the neck diameter, and the larger the neck diameter, the more remarkable. In addition, the shift of the peak of the absorption coefficient at f_h is about the same under any conditions. In the random incident absorption coefficient, since the weight of the incident angle 45° is the largest at the time of total averaging, the peak on the bass region side

can be seen around f_{lh} at about 45° incident angle. When the shift of the resonance frequency due to the incident angle is small (a ~ d), the peak value is also approximated to the value at 45° incidence. BPHP is characterized in that even if the back air-layer is very narrow, plate resonance absorption equivalent to the PHP thickness can be obtained. At that time, it is easy to apply, because the peak frequency of the absorption coefficient at random incidence is almost the same as that at normal incidence. On the other hand, when the shift is large (e ~ f), there is a tendency to slightly broaden the bandwidth.

4.2 Discussion on panel design and installation

Based on the same parameter settings in Section 3.2 as a basic condition, a plurality of parameters was changed to calculate peak values and peak Q values of the normal-incident absorption coefficient at the resonance frequency f_l on the low frequency range. The frequency at which the absorption coefficient is a half value of the peak value is difficult to express explicitly from the equation (1) ~ (3), so it was calculated by iterative calculation by iterative method. When the half width is 1/D octave band width, the Q value is about 1.41D. After that, assuming three situations, we will consider the design and installation of the BPHP.

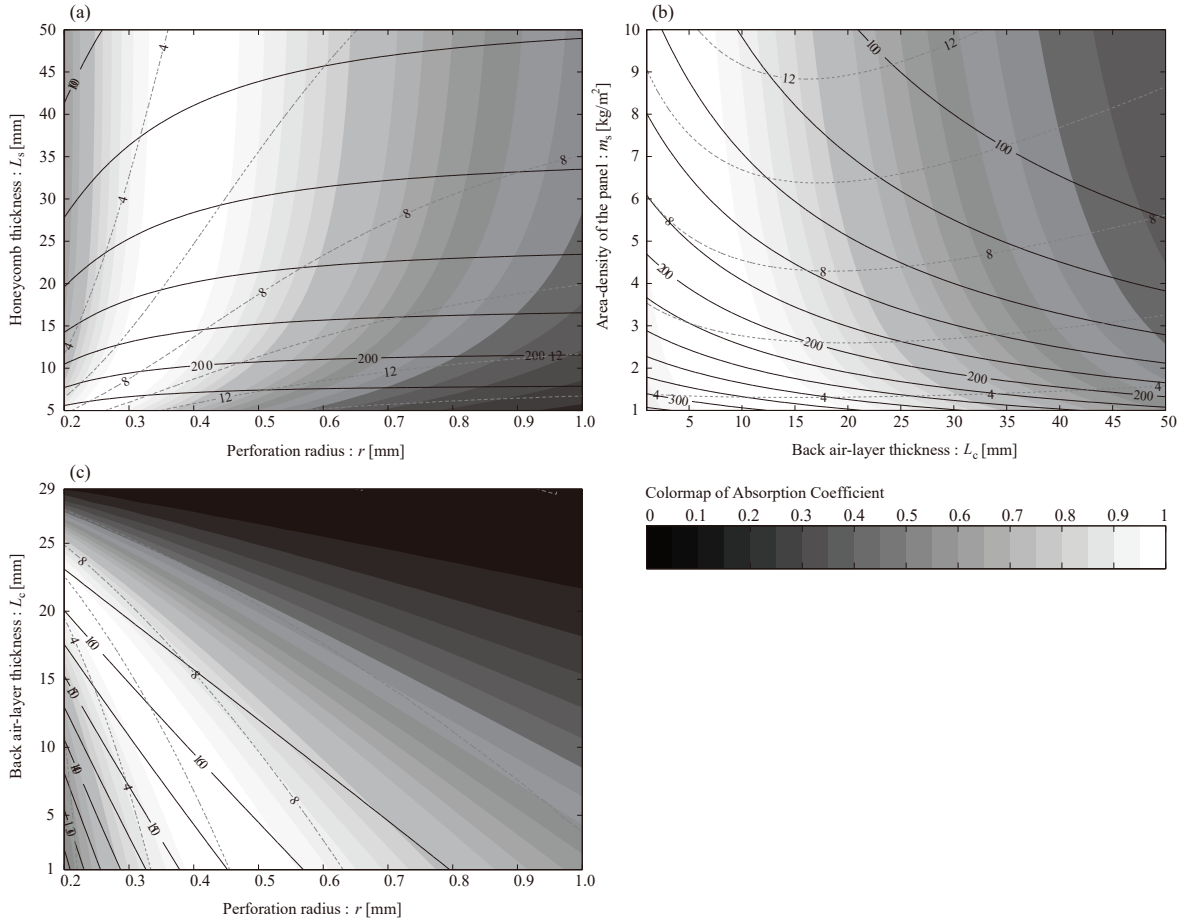

Figure 6 – Absorption coefficient at the eigen-frequency, f_l, calculated with changing (a) L_s and r, (b) m_s and L_c and (c) L_s, L_c and r under the total depth $L_s + L_c = 30$ mm. (Solid and dotted contour lines are drawn for f_l and Q factor, respectively.)

4.2.1 Higher performance of panels

Figure 6(a) shows the result when changing panel thickness L_s and hole radius r. Although the change of the resonance frequency according to the hole radius is slight, the absorption coefficient becomes large at a hole radius of about 0.3 mm ~ 0.4 mm. Also, as the L_s is larger, the resonance frequency can be designed to be in the low frequency range, and the Q value can be further reduced.

4.2.2 Installation of existing panels

Figure 6(b) shows the results when changing the back air-layer thickness L_c and the panel surface

density m_s. Even if L_c is about 1 mm, the absorption coefficient is very large, and it can be installed in close contact with the back wall. It is possible to lower the resonance frequency by increasing L_c, m_s. However, when L_c is increased, the change in Q value is small but the peak value is small. Conversely, when m_s is increased, the change in peak value is small but the Q value is large.

4.2.3 When there is a restriction in the additional thickness

Figure 6(c) shows the results when changing the panel thickness L_s, the back air-layer thickness L_c and the hole radius r. However, the distance from the panel surface to the back wall (the sum of L_s and L_c) is constant at 30 mm. Under this condition, it can be seen that the contours of the absorption coefficient, the resonance frequency, and the Q value change nearly in parallel. In addition, it is difficult to considerably change the resonance frequency in the range where the absorption coefficient is large. Therefore, it is considered that setting a parameter having a high absorption coefficient and a low Q value allows absorption coefficient to the lower frequency range. As an example, in the case of Ls = 10 mm, L_c = 20 mm, r = 0.2 mm, the resonance frequency is 160 Hz, the absorption coefficient is 1, and the Q value is 4 or so. At this time, absorption coefficient of 0.5 or more can be obtained within the half width (140 Hz ~ 180 Hz).

5. CONCLUSIONS

In this paper, we constructed a simple theoretical model with lumped constant system to calculate the absorption coefficient for the BPHP. As a result of comparing the normal incidence absorption coefficient with the lumped constant model and the detailed model by the finite element method, it was confirmed that both corresponded well. After that, through parametric studies, we summarized the characteristics of the oblique-incidence and random-incidence absorption coefficients, and foundational absorption performance design. Verification by actual measurement is required in the future.

REFERENCES

1. M. Toyoda, M. Tanaka and D. Takahashi, Reduction of acoustic radiation by perforated board and honeycomb layer system, Appl. Acoust., 68, 71-85 (2007)
2. M. Toyoda and D. Takahashi, Sound transmission through a microperforated-panel structure with subdivided air cavities, J. Acoust. Soc. Am, 124, 3594-3603 (2008)
3. M. Toyoda, K. Sakagami, D. Takahashi and M. Morimoto, Effect of a honeycomb on the sound absorption characteristics of panel-type absorbers, Appl. Acoust., 72, 943-948 (2011)
4. J.F. Allard and N. Atalla, Propagation of sound in porous media, 2nd ed., Wiley (2009)